SIAM J. APPL. MATH.
Vol. 62, No. 3, pp. 853–869
© 2001 Society for Industrial and Applied Mathematics

FINGER FORMATION IN BIOFILM LAYERS*

J. DOCKERY† AND I. KLAPPER†

Abstract. A simple single substrate limiting model of a growing biofilm layer is presented. One-dimensional moving front solutions are analyzed. Under certain conditions these solutions are shown to be linearly unstable to fingering instabilities. Scaling laws for the biofilm growth rate and length scale are derived. The nonlinear evolution of the fingering instabilities is tracked numerically using a level set method, leading to the observation of mushroom-like structures.

Key words. biofilms, fronts, fingering instability

AMS subject classifications. Primary, 92C15; Secondary, 76Z99

PII. S0036139900371709

1. Introduction.

A biofilm is a substance composed of millions of microorganisms (bacteria, fungi, algae, and protozoa) that accumulate on surfaces in flowing aqueous environments (Figure 1). These film-forming microorganisms secrete extracellular polymers which anchor the cells to each other as well as to the surfaces on which the film is formed. Once anchored to a surface, biofilm microorganisms carry out a variety of detrimental or beneficial reactions, depending on the surrounding conditions. For an overview of the biofilm process see [9].

An important characteristic of these complex ecological systems is that they can have a significant impact on the surrounding environment. Some of the effects associated with biofilm formation include biofouling (fouling or contamination linked to microbial activity), biocorrosion (especially of industrial pipes), oil field souring (reduction of sulfates by microbes in soil), and infections caused by biofilm growth on host tissues or medical implants. Not all biofilm activity has negative results. Bacteria within biofilms can break down contaminants in soil and water and are often used for remediation purposes such as waste water treatment (see [15]).

While there has been considerable quantitative study of suspended cell cultures and of pattern formation in various types of tissues, relatively little mathematical attention has been paid to biofilms. In contrast, within the microbiology community biofilm research is becoming an increasingly active area, as researchers recognize that attached organisms often predominate in a wide range of medical, natural, and industrial environments. Effective biofilm models could be a fast and cost-effective aid for biologists.

Biofilm models are generally based on three principle elements. First, they must incorporate some kind of transport mechanisms (diffusion, advection) for bringing nutrients to the active material in the biofilm (or removing waste, delivering chemical signals, etc.). Typically, transport is handled using a steady state diffusion or advection-diffusion equation, under the assumption that the biofilm evolves very slowly relative to most transport time-scales. Second, biofilm models usually require some consumption and growth mechanisms. The simplest models restrict this activity to the

*Received by the editors May 1, 2000; accepted for publication (in revised form) February 5, 2001; published electronically December 28, 2001.

http://www.siam.org/journals/siap/62-3/37170.html

†Department of Mathematical Sciences, Montana State University, Bozeman, MT 59717 (umsfjdoc@math.montana.edu, klapper@math.montana.edu). The research of the first author was supported by NSF DMS-9805701. The research of the second author was supported by NSF DMS-9704486.

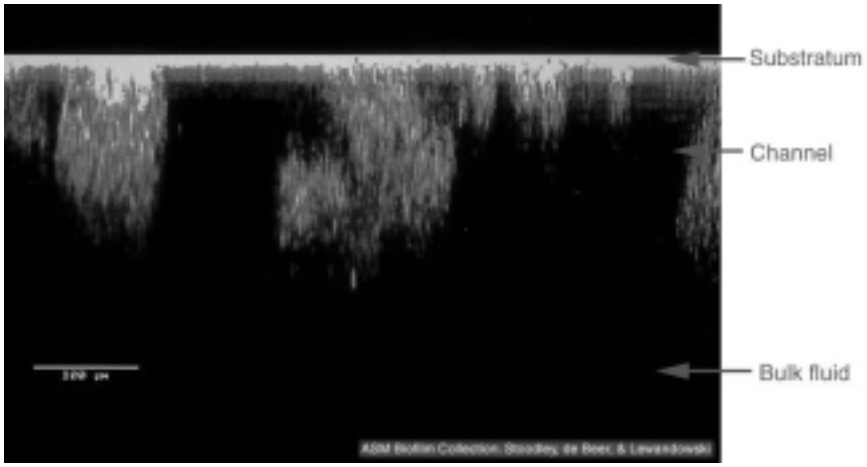

FIG. 1. *Cross-sectional view of a typical biofilm. Image supplied by P. Stoodley and available from the ASM Biofilms Collection at http://www.microbelibrary.org/images/biofilms/annotated/*012*a.jpg.*

biofilm interface [26]. More recently, cellular automaton (CA) and partial CA models [16, 21, 20] have allowed for interior activity, albeit in a somewhat ad hoc manner. These models are similar in spirit to some previous models of pattern formation in bacteria [3]. We present here a continuum model of both growth and consumption. A rather different continuum model is presented in [12]. The third important but problematic element of a biofilm model is mechanisms for biofilm necrosis and loss. This aspect of biofilm activity is a currently active area of experimental study, and understanding remains limited. Previous CA and analytical models have included apparently arbitrary effects—surface scraping, for example—for the purpose of producing a steady state. Recently, attempts have been made to include the elastic reaction of biofilms to fluid stress, including biofilm sloughing [20]. Fluid stress has also been included in microscale biofilm simulations [11]. We will assume negligible fluid stress here. For computational convenience, we will include deep layer necrosis (similar to that used in avascular tumor models, e.g., [13]) to prevent our biofilm from growing out of its computational box.

Another interesting and important feature of biofilms is their complicated internal structure. Recent improvements in microscopy and imaging techniques have resulted in the realization that most biofilms are not as uniform as once thought [24, 10]; see, for example, Figure 1. The cause of this heterogeneity is another of the basic open questions in biofilm research. Is heterogeneity an internal mechanical effect? What is the influence of external hydrodynamic stress? Is it possible for cell-cell communication through chemical signaling to be responsible for some of the heterogeneity? Can species competition be a contributing factor in the roughness that one observes? What role does detachment have on biofilm structure and vice versa? Understanding the variations in biofilm structure will help us understand issues of transport and chemistry within the biofilm. It may turn out that there are situations where the heterogeneity is unimportant and existing models would be sufficient, but this is difficult to ascertain without comparison to models that are capable of producing heterogeneous biofilms and, crucially, comparison with experimental data.

There are many similarities between biofilm modeling and other areas of mathe-

matical biology, for example, modeling of tumor growth (e.g., [13, 5, 4]), modeling of morphogenesis in various situations [1, 18], modeling of pattern formation of bacterial colonies grown on an agar substrate [3], and wall growth models for the gut [2]. In addition, there are many other physical problems that have long been characterized by similar unstable moving boundaries [22, 7, 17], for example, crystal growth, Hele–Shaw flow, diffusion-limited aggregation, etc. See [19] for a general overview. The biofilm model presented here provides another variation on these widely familiar examples.

In this paper we present a simple model of a single substrate limited biofilm growing into a static aqueous environment. The model equations are derived in section 2. The model is essentially solvable in one dimension, and this solution is presented in section 3. In section 4 it is shown that these one-dimensional (1D) planar front solutions are linearly unstable to two-dimensional (2D) and three-dimensional (3D) perturbations under certain circumstances. In section 5 the full nonlinear evolution of these instabilities is followed numerically in two dimensions.

2. The biofilm model. We divide R^3 into a biofilm region $z < h(x, y, t)$ and an aqueous region $z > h(x, y, t)$, with interface surface $z = h(x, y, t)$. (More generally, the interface at any given time need not be expressible as a function of x and y.) The biofilm is modeled as a homogeneous, viscous, incompressible fluid of constant density, satisfying Darcy's law

$$\mathbf{u} = -\lambda \nabla p$$

for some constant λ ($\mathbf{u}$ is velocity and p is pressure). Despite incompressibility, the biofilm may be growing (or decaying) at any given location so that effectively the biofilm fluid contains a field of sources (or sinks). Thus

$$\nabla \cdot \mathbf{u} = g \tag{2.1}$$

for some prescribed *growth function* g. Hence

$$-\lambda \nabla^2 p = g. \tag{2.2}$$

The normal velocity of the biofilm interface $(x, y, h(x, y, t))$ is $-\mathbf{n} \cdot \lambda \nabla p|_{z=h^-}$, where $\mathbf{n}$ is the unit upward normal and h^- indicates that z should approach h from below, the biofilm side. From (2.2) it is evident that p is proportional to λ^{-1}, and hence the interface velocity is independent of λ. This fact can be understood by observing that the speed of motion of the interface is determined by conservation of mass and biofilm generation (or decay) and hence depends on g but not λ.

We assume that the aqueous region $z > h$ is static near the biofilm and hence that the pressure is constant there. In fact, we set $p = 0$ for $z > h$. Implicit in this assumption is the expectation that the biofilm interface evolves quasi-statically, since the typical biofilm evolution time is on the order of hours. With $p = 0$ for $z > h$ we obtain boundary conditions $p|_{z=h} = 0$ and $p_z|_{z=-\infty} = 0$ for (2.2).

The growth function g is determined by local conditions in the biofilm and also, in principle, by the biofilm history. For simplicity we assume, however, that g depends only on the concentration $S(x, y, z, t)$ of a single limiting substrate, e.g., oxygen or glucose. In particular, we assume that $g = g(u(S))$, where u, the *usage function* or *substrate uptake rate*, indicates the rate of substrate usage. Note that u and g do not depend explicitly on time or space in the model presented here. A typical choice for

$u(S)$ is the function

$$u(S) = u_{max}\frac{S}{S+K_S},$$

sometimes called the Monod function. The parameters u_{max} and K_S are the maximum usage and half-saturation, respectively. This form is also often used for the growth function g. In particular, frequently $g(S) \propto u(S)$.

Substrate diffuses through the aqueous region into the biofilm, where it also diffuses and is consumed. We assume that there is a function $H(x,y,t)$ with $H \geq h$ such that, for $z \geq H$, the substrate amplitude is constant, i.e., for $z \geq H$, $S(x,y,z,t) = S_\infty$. This assumption is meant to model a bulk flow region away from the biofilm, where the substrate is constantly replenished.

Hence we obtain the substrate equations

$$\begin{aligned} &S_t - D_1\nabla^2 S = 0, \qquad h < z < H, \\ &S_t - D_2\nabla^2 S = -u(S), \quad z < h, \end{aligned} \tag{2.3}$$

with boundary conditions $S|_{z=H} = S_\infty$, $S_z|_{z=-\infty} = 0$, and matching conditions $S|_{z=h^+} = S|_{z=h^-}$, $D_1\nabla S|_{z=h^+} = D_2\nabla S|_{z=h^-}$. Here again, $h^\pm$ refers to z approaching h from above or below, respectively. We remark that the time derivatives S_t appearing in (2.3) are in fact advective derivatives. As was previously noted and will again be argued below, however, advective terms can be neglected here due to the slow evolution of the system. Thus S can be considered to evolve quasi-statically.

Equations (2.2) and (2.3), together with their boundary conditions, comprise the biofilm model to be studied in this paper. Before proceeding, we scale and nondimensionalize as follows. Introduce the horizontal system width w (e.g., the horizontal box size). The quantity $S_\infty/u(S_\infty)$ is a substrate consumption rate near the top of the biofilm, and thus the substrate penetration depth $\ell_S = (D_2 S_\infty/u(S_\infty))^{1/2}$ measures the distance substrate is able to diffuse into the biofilm before being consumed. (The biofilm layer to depth $z = h - \ell_S$ is sometimes called the *active layer*.) Also introduce the system time scale T measuring the time scale for the biofilm to evolve an $O(w)$ amount. Then setting $\tilde{\mathbf{x}} = \mathbf{x}/w$, $\tilde{h} = h/w$, $\tilde{H} = H/w$, $\tilde{t} = t/T$, $\tilde{S} = S/S_\infty$, $\tilde{u} = u/u(S_\infty)$, $\tilde{g} = gS_\infty/u(S_\infty)$, and $\tilde{p} = pG^{-1}\nu\lambda/D_2$, we obtain the nondimensional system (after dropping the tildes)

$$\begin{aligned} &\nabla^2 p = -g(u(SS_\infty)), \qquad z < h, \\ &\epsilon_1 S_t - \nabla^2 S = 0, \qquad h < z < H, \\ &\epsilon_2 S_t - \nabla^2 S = -Gu(SS_\infty), \quad z < h, \end{aligned} \tag{2.4}$$

with interface velocity $-\mathbf{n}\cdot\nabla p_{z=h^-}$. Here $G = w^2/\ell_S^2 = w^2 u(S_\infty)/D_2 S_\infty$ is the nondimensional growth number, $\nu = TS_\infty/u(S_\infty)$ is the nondimensional ratio of the system growth and substrate evolution times, and $\epsilon_i = w^2/D_i T$ are nondimensional numbers comparing system diffusion times to the system evolution time. Estimating $D_i \approx 10^{-9} m^2/s$ and, conservatively, $T = 10^5 s$ (see [14]), ϵ_i can be considered small for biofilm length scales up to about $10^4 \mu$m, well within observable levels. We hence set $\epsilon_1 = \epsilon_2 = 0$. Also henceforth we replace $u(SS_\infty)$ by $u(S)$, absorbing S_∞ into u. The nondimensional number $G^{-1/2}$ is a relative measure of the depth of the biofilm active layer and will be seen to be a controlling parameter. This parameter has already been observed numerically to be important in CA models [21].

The boundary and matching conditions for (2.4) are (when $\epsilon_1 = \epsilon_2 = 0$) $p|_{z=h} = 0$, $p_z|_{z=-\infty} = 0$, $S|_{z=H} = 1$, $S_z|_{z=-\infty} = 0$, $S|_{z=h^+} = S|_{z=h^-}$, and $K\nabla S|_{z=h^+} \cdot \mathbf{n} = \nabla S|_{z=h^-} \cdot \mathbf{n}$, where $K = D_1/D_2$. As a final remark, in addition to (2.4) we require on physical grounds that $S \geq 0$. To enforce this it may be necessary for some choices of $u(S)$ to introduce a third layer $z < \bar{h} < h$, where S is identically 0.

3. The 1D problem. We begin by assuming that the quantities S, p, h, and H are functions only of z and t so that (2.4) becomes

$$\begin{aligned} p_{zz} &= -g(u(S)), \qquad z < h(t), \\ S_{zz} &= \begin{cases} 0, & h(t) < z < H(t), \\ Gu(S), & z < h(t), \end{cases} \end{aligned} \tag{3.1}$$

together with the interface evolution equation

$$\dot{h} = -p_z|_{z=h^-}.$$

We assume $H(t) = h(t) + L$ for a given constant L. The boundary and matching conditions for (3.1) are as before.

To solve for $S(z,t)$, we first note that

$$S(z,t) = 1 + A(z - (h+L)), \quad h < z < h + L,$$

for some constant A to be determined. By manipulating the matching conditions at $z = h$ it becomes apparent that for $z < h$ we must solve

$$S_{zz} = Gu(S), \quad S_z(-\infty, t) = 0, \quad S(h,t) + LK^{-1}S_z(h,t) = 1. \tag{3.2}$$

(We then also obtain $A = K^{-1}S_z(h,t) = L^{-1}(1 - S(h,t))$.)

At this point, it becomes necessary to place some restrictions on the function $u(S)$ defined for $S \geq 0$. First, we require $u(0) = 0$ and $u(S) > 0$ for $S > 0$. (If no substrate is present then none is used, and substrate usage is always positive if substrate concentration is positive.) Second, for convenience we assume the nondegeneracy condition $u'(0) > 0$. Third, again essentially for convenience, we assume that $u(S)$ is Lipschitz continuous on $S \geq 0$.

Under these conditions we claim that (3.2) has a unique solution $S(z,t)$. Furthermore, this solution has the following properties: $S(z,t)$ and $S_z(z,t)$ are positive and monotone increasing with $S(-\infty, t) = 0$, $0 < S(z,t) < 1$, $0 < S_z(z,t) < L^{-1}K$, and $S(z,t) \sim \exp(\sqrt{Gu'(0)}z)$ as $z \to -\infty$. The depth of the region where S is $O(1)$ is $O(G^{-1/2})$. Also, notably, the concentration profile $S(z,t)$ is independent of time, in the sense that $S(z,t) = S(z - (h(t) - h(0)), 0)$.

To verify the claim, we study (3.2) at fixed t in the phase space of the variables $S(z)$ and $Q(z) = S_z(z)$. S and Q satisfy the system

$$\begin{aligned} \dot{S} &= Q, \\ \dot{Q} &= Gu(S). \end{aligned} \tag{3.3}$$

Since u is Lipschitz, this system, considered as an initial value problem, has global unique solutions (except when trajectories arrive at the axis $S = 0$ at finite time). To solve the problem (3.2) we need to find a trajectory that starts on the line $S + LK^{-1}Q = 1$, with $S > 0$ at $z = h$, and arrives at the S axis at $z = -\infty$ (see Figure 2).

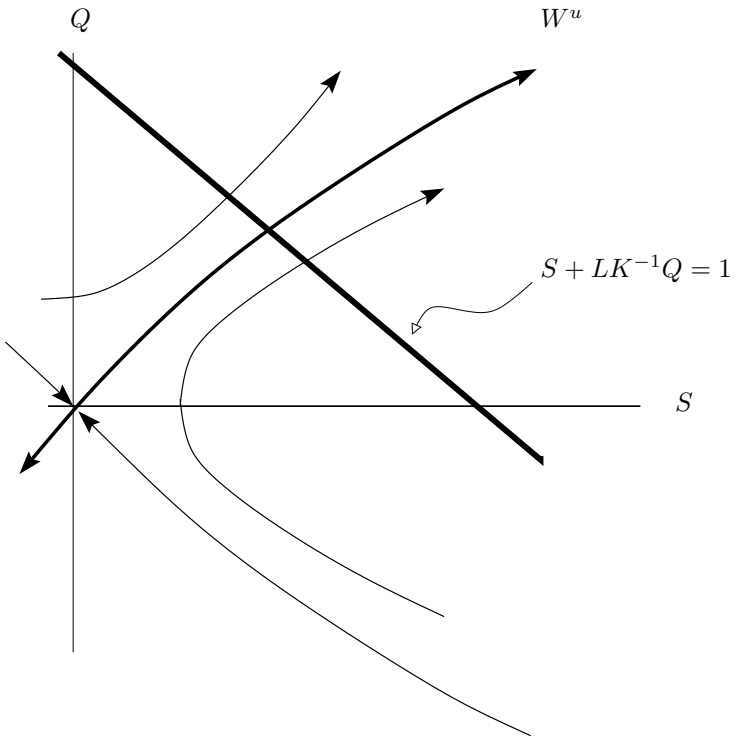

FIG. 2. *Schematic diagram showing the phase plane.*

It is easily seen that the only fixed point of (3.3), namely $(0,0)$, is a saddle with unstable eigenvector $(1, \sqrt{Gu'(0)})$ and stable eigenvector $(1, -\sqrt{Gu'(0)})$. Since $\dot{Q} = u(S) \geq 0$ on $S \geq 0$, and $\dot{S} = Q$ is positive for $Q > 0$ and negative for $Q < 0$, then the system trajectories must appear as in Figure 2. Clearly the trajectory starting at $z = h$ from the intersection of the unstable manifold with the line $S + LK^{-1}Q = 1$ arrives at the origin at $z = -\infty$. Trajectories starting below the intersection on the line $S + LK^{-1}Q = 1$ go to infinity as $z \to -\infty$, and trajectories starting above the intersection on the line $S + LK^{-1}Q = 1$ reach $S = 0$ at finite z with $S_z > 0$ and hence cannot be matched to a 0 solution.

Furthermore, we can make the following observations. First, the constructed solution to (3.3) is independent of time in the sense described above, i.e., changing h merely amounts to reparametrizing the solution trajectory. Second, near the origin, (3.3) is well approximated by the linearization

$$\begin{aligned} \dot{S} &= Q, \\ \dot{Q} &= Gu'(0)S, \end{aligned}$$

so that we observe that the solution trajectory has the property that $S \sim \exp[\sqrt{Gu'(0)}z]$ as $z \to -\infty$. Third, the solution trajectory stays in the first quadrant below the line $S + LK^{-1}Q = 1$, verifying $0 < S(z) < 1$, $0 < S_z(z) < L^{-1}K$. In fact, both $S(z)$ and $S_z(z)$ are monotone decreasing as $z \to -\infty$. Finally, by rescaling (3.3) we observe that the size of the region $S > c$ for any c is $O(G^{-1/2})$. We will refer to the region where S is $O(1)$ as the active region.

Given a solution S to the substrate equations, we can now solve the pressure equation in (3.1) to obtain

$$p(z,t) = \int_z^{h(t)} \int_{-\infty}^{r} g(\eta,t)d\eta dr,$$

where we have written $g(u(S(z,t))) = g(z,t)$. Since S, and hence $u(S)$, decays exponentially as $z \to -\infty$, this integral will converge as long as $g(u) \to 0$ sufficiently quickly as $u \to 0$ (for example, linearly). This is essentially the only condition placed on g. Given convergence, then

$$\dot{h}(t) = -p_z(h(t),t) = \int_{-\infty}^{h(t)} g(s,t)ds.$$

As should be expected, the biofilm interface moves to exactly accomodate the volume $\int_{-\infty}^{h(t)} g(s,t)ds$ of newly generated biofilm. We remark as well that due to the invariance property of S under change of h, the integral $\int_{-\infty}^{h(t)} g(s,t)ds$ is a constant independent of time. Hence the biofilm interface advances at a constant speed, roughly $G^{-1/2}g|_{z=h} \sim G^{-1/2}g(1)$, the depth of the active region times the approximate growth rate at the top of the biofilm. We stress that the above analysis places only weak conditions on the biology functions u and g and hence is, roughly speaking, independent of the biological details of a given specific biofilm system.

As a particular example, we choose u and g to be (in scaled variables) the linear functions

$$u(S) = S, \quad g(u) = \alpha u = \alpha S.$$

In fact, α can be scaled into the pressure p and hence effectively only rescales time. We thus set $\alpha = 1$. Solving (3.2) we obtain

$$S(z,t) = \begin{cases} 1 - \dfrac{\sqrt{G}}{K}\left(\dfrac{1}{1+K^{-1}L\sqrt{G}}\right)(h+L-z), & h < z < h+L, \\ \dfrac{1}{1+K^{-1}L\sqrt{G}}\exp[-\sqrt{G}(h-z)], & z < h. \end{cases} \tag{3.4}$$

Note that the substrate S is concentrated in a layer of thickness $G^{-1/2}$ at the top of the biofilm.

Next, solving the pressure equation we obtain

$$p(z,t) = \frac{1}{G}\left(\frac{1}{1+K^{-1}L\sqrt{G}}\right)(1-\exp[-\sqrt{G}(h-z)]), \tag{3.5}$$

leading to the interface equation

$$\dot{h} = -p_z(h,t) = \frac{1}{\sqrt{G}}\left(\frac{1}{1+K^{-1}L\sqrt{G}}\right). \tag{3.6}$$

Note that the right-hand side is exactly the constant $G^{-1/2}g|_{z=h}$ and hence, as expected, h increases linearly in time.

4. Linear analysis of the fingering instability. In order to study the linear stability of the moving front solution of the previous section, we now consider solutions to (2.4) (with, as always, $\epsilon_1 = \epsilon_2 = 0$) of the form

$$\begin{aligned} S(x,y,z,t) &= S_0(z,t) + S_1(z,t)\exp(i\mathbf{k}\cdot\mathbf{x}), \\ p(x,y,z,t) &= p_0(z,t) + p_1(z,t)\exp(i\mathbf{k}\cdot\mathbf{x}), \\ h(x,y,t) &= h_0(t) + h_1(t)\exp(i\mathbf{k}\cdot\mathbf{x}), \end{aligned} \tag{4.1}$$

where $\mathbf{k} = 2\pi(k_x, k_y) \neq (0,0)$, $\mathbf{x} = (x,y)$, and S_0, p_0, and h_0 are the one-dimensional front solutions found in the previous section. In order to linearize, it is necessary to assume that the quantities kS_1, kp_1, and kh_1 are sufficiently small, where $k^2 = k_x^2 + k_y^2$. Also, there is again some choice in where to place the upper boundary H. For simplicity, we set $H(x,y,t) = h_0(t) + L$, where L is a given constant (as in the previous section). Note that S_1, p_1, and h_1 may be complex. When mentioning these quantities below, it is always implicit that only real parts are to be considered.

We now plug (4.1) into (2.4) and, combining the result with the interface velocity $-\mathbf{n}\cdot\nabla p|_{z=h^-}$, attempt to solve to first order, looking for growing modes. We remark that, to first order,

$$\mathbf{n} = \hat{\mathbf{z}} + \exp(i\mathbf{k}\cdot\mathbf{x}) \begin{pmatrix} -2\pi i k_x h_1 \\ -2\pi i k_y h_1 \\ 0 \end{pmatrix}, \tag{4.2}$$

where $\hat{\mathbf{z}}$ is a unit vector in the z direction. From the substrate equation we obtain

$$S_{1,zz} = \begin{cases} k^2 S_1, & h_0 < z < h_0 + L, \\ (k^2 + Gu'(S_0(z,t)))S_1, & z < h_0. \end{cases}$$

Using the previous remark about the normal vector, the boundary conditions are

$$S_1(h_0 + L, t) = S_{1,z}(-\infty, t) = 0,$$

with interface conditions

$$\begin{aligned} h_1 S_{0,z}(h_0^+, t) + S_1(h_0^+, t) &= h_1 S_{0,z}(h_0^-, t) + S_1(h_0^-, t), \\ K S_{1,z}(h_0^+, t) &= h_1 S_{0,zz}(h_0^-, t) + S_{1,z}(h_0^-, t). \end{aligned}$$

From these boundary and matching conditions it follows that

$$S_1(z,t) = A(t)\sinh[k(h_0 + L - z)], \quad h_0 < z < h_0 + L,$$

for some function $A(t)$, and that for $z < h_0$,

$$S_{1,zz} = (k^2 + Gu'(S_0(z,t)))S_1, \tag{4.3}$$

with boundary conditions

$$S_{1,z}(-\infty, t) = 0, \tag{4.4}$$

$$S_1(h_0, t) + (kK)^{-1}\tanh(kL) S_{1,z}(h_0, t) = \beta h_1, \tag{4.5}$$

where $\beta = -[(kK)^{-1}\tanh(kL)Gu(S_0(h_0,t)) + (1 - K^{-1})S_{0,z}(h_0^-, t)]$ is known from the 1D solution. After solving (4.3) we can then recover $A(t) = -(kK\cosh(kL))^{-1}$ $\cdot(Gu(S_0(h_0^-, t))h_1 + S_{1,z}(h_0^-, t))$.

Equation (4.3) is very similar to (3.2) although it is linear. Other notable differences are, first, that S_1 may be allowed to be negative and, second, that if the perturbation $h_1 > 0$ then the right-hand side of (4.5) is negative because in the relevant case of $K = D_1/D_2 \geq 1$, we obtain $\beta < 0$.

It is easy to show that the linear boundary value problem in (4.3)–(4.5) has a unique solution. Indeed, it follows from standard results [8, Chapter 3] that (4.3) has a unique solution $\psi(x)$ satisfying $\lim_{z\to-\infty}\psi(z)e^{-\gamma z} = 1$ and $\lim_{z\to-\infty}\psi'(z)e^{-\gamma z} = \gamma$, where $\gamma = \sqrt{k^2 + Gu'(0)}$. Since (4.3) is linear, we see that any solution of (4.3)–(4.4) must be a constant multiple of ψ. It follows then that the solution of (4.3)–(4.5) is given by $S_1 = \alpha\psi$, where

$$\alpha = \frac{\beta h_1}{\psi(h_0) + (kK)^{-1}\tanh(kL)\psi'(h_0)}.$$

In addition, we note the properties that (for $h_1 > 0$) $\beta h_1 < S_1(z,t) < 0$ and $(kK/\tanh(kL))\beta h_1 < S_{1,z}(z,t) < 0$ (the inequalities are reversed if $h_1 < 0$).

Next we require that, to first order, $p(x,y,z,t)$ satisfies

$$\nabla^2 p = -g, \quad y < h(x,t)$$

with boundary conditions $p_z(x,y,-\infty,t) = p(x,y,h,t) = 0$. Hence

$$p_{1,zz} - k^2 p_1 = -g_1,$$

where $g_1(z,t) = Dg(u(S_0(z,t)))S_1(z,t)$, with boundary conditions

$$p_{1,z}(-\infty,t) = 0,$$
$$p_1(h_0,t) = -p_{0,z}(h_0,t)h_1 = h_1\int_{-\infty}^{h_0(t)} g_0(s,t)ds,$$

where $g_0(z,t) = g(u(S_0(z,t)))$. This equation has explicit solution

$$p_1(z,t) = \exp[k(z-h_0)]\left(k^{-1}\int_{-\infty}^{h_0} g_1(s,t)\sinh[k(h_0-s)]ds + h_1(t)\int_{-\infty}^{h_0} g_0(s,t)ds\right)$$
$$-k^{-1}\int_{-\infty}^{z} g_1(s,t)\sinh[k(z-s)]ds.$$

To complete the calculation, we obtain an equation for $h_1(t)$ by recalling that the normal interface velocity is given by $-\mathbf{n}\cdot\nabla p|_{y=h^-}$. Using (4.2) we find that to first order

$$-\mathbf{n}\cdot\nabla p|_{z=h} = -\hat{\mathbf{z}}\cdot\nabla p|_{z=h}$$
$$= \int_{-\infty}^{h_0} g_0(s,t)ds + \exp(i\mathbf{k}\cdot\mathbf{x})\left[h_1(t)g_0(h_0,t) - p_{1,z}(h_0,t)\right],$$

and also to first order

$$-\mathbf{n}\cdot\nabla p|_{z=h} = -\hat{\mathbf{z}}\cdot\nabla p|_{z=h} = \dot{h} = \dot{h}_0 + \dot{h}_1\exp(i\mathbf{k}\cdot\mathbf{x}),$$

with the result that

$$\dot{h}_1 = h_1\left[g_0(h_0,t) - k\int_{-\infty}^{h_0} g_0(s,t)ds\right] + \int_{-\infty}^{h_0} g_1(s,t)\exp[-k(h_0-s)]ds. \tag{4.6}$$

If we assume that u and g are smooth and thus $Dg(u(S_0(z,t)))S_1(z,t)$ approaches zero as $z \to -\infty$ (where $S_0, S_1 \to 0$), then the last integral in (4.6) converges since $S_1 \sim \exp[\sqrt{k^2 + Gu'(0)}z]$ as $z \to -\infty$. We also remark that this integral is linear in h_1 since g_1 is linear in h_1; hence (4.6) can be written as $\dot{h}_1 = \omega(k)h_1$ for some function $\omega(k)$.

The right-hand side of (4.6) consists of two terms that influence the evolution of the perturbed biofilm interface essentially in competitive ways. The first term (in brackets) contains the zeroth order growth effect on the first order interface perturbation. This component of the dispersion relation is linear in k, becoming negative for k larger than

$$k_{crit} = g_0(h_0,t)\left[\int_{-\infty}^{h_0} g_0(s,t)ds\right]^{-1} = O(G^{1/2}).$$

At $k = k_{crit}$, the perturbation length scale is approximately the same as the active layer depth. For $k < k_{crit}$, the active layer does not really distinguish the perturbed interface from the flat, zeroth order interface and hence will tend to amplify the perturbation right along with the original biofilm surface. For $k > k_{crit}$, however, the active layer depth is large compared to the perturbation length scale, and in this case the active layer is able to distinguish fingering perturbations. Growth-generated pressure from below pushes preferentially on perturbation troughs, thus damping short wavelength fingering.

The second term in (4.6) contains the contribution to fingering from the effects of first order corrections to the growth profile on the zeroth order interface. Intuitively, this term reflects the advantage of biofilm protrusions upward into substrate-rich regions and hence favors finger growth. However, we note that, somewhat nonintuitively, this second term is negative (since $g_1(z,t) = Dg(u(S_0(z,t)))S_1(z,t)$ is negative). So in fact this term opposes all perturbations. But high values of k are less adversely affected than low values, as can be seen as follows. It is easily observed that $g_1(z,t)$ decays exponentially for values of z below the active layer, since both S_0 and S_1 decay exponentially there, while on the other hand the exponential $\exp[-k(h_0 - s)]$ favors contributions from the biofilm layer of depth k^{-1} below $z = h$. Hence it can generally be expected that the second term will decay like k^{-1} for values of $k > G^{1/2}$, and so the second term in (4.6) will be small for large k. In the case $k < G^{1/2}$, however, we would then expect the exponential to be unimportant, and so

$$\int_{-\infty}^{h_0} g_1(s,t)\exp[-k(h_0 - s)]ds \sim g_1(h_0,t)G^{-1/2}$$

for large G. The size of this integral will depend on details of the functions u and g as $g_1(z,t) = Dg(u(S_0(z,t)))S_1(z,t)$, but it can be expected that, in the low S case, Dg will be $O(G^{1/2})$ throughout the active layer. So if $S_1(h_0,t)$ is sufficiently large, then the second term in (4.6) will suppress low-k perturbations to a sufficiently greater extent than high-k perturbations, such that, in combination with the first term in (4.6), a fingering instability will result. Moreover, the preferred wavelength of this instability should be $O(G^{-1/2})$. The magnitude of $S_1(h_0,t)$ depends on details of the active layer in a complicated way, so that it seems difficult to find a simple condition on u, g, and the various parameters that can discriminate between fingering and nonfingering regimes.

We make the following important remark, however. If we assume, regardless of choice of u and g, that, for sufficiently low values of S, $u(S) \sim u'(0)S$, $g(S) \sim g'(0)S$,

with $u'(0) > 0$, $g'(0) > 0$, then we will observe shortly that the model is able to exhibit linear instability at sufficiently low S for general choice of biology functions. The fact that biofilms seem to be prone to fingering at low levels of the rate-limiting substrate would seem to indicate that the linear example is in fact the relevant regime in the present context.

We thus return to the choice $u(S) = S$, $g(u) = u = S$, considered in the previous section. In this case, $S_0(z,t)$ and $p_0(z,t)$ are given by (3.4) and (3.5), respectively, and $h_0(t)$ is the solution to (3.6). Then for $z < h_0(t)$, $S_1(z,t)$ is the solution to

$$S_{1,zz} = \begin{cases} k^2 S_1, & h < z < h + L, \\ (k^2 + G)S_1, & -\infty < z < h. \end{cases}$$

Using the boundary and interface conditions we obtain

$$S_1(z,t) = \begin{cases} C_U \bar{S}_I \sqrt{G} \frac{\sinh[k(h+L-z)]}{\cosh[kL]} h_1(t), & h < z < h + L, \\ C_L \bar{S}_I \sqrt{G} \exp[-\kappa(h-z)] h_1(t), & -\infty < z < h, \end{cases}$$

where $\kappa^2 = k^2 + G$, $\bar{S}_I = (1 + K^{-1} L\sqrt{G})^{-1}$, and

$$C_U(k) = \frac{-k^{-1}\sqrt{G} + (1 - K^{-1})}{Kk\kappa^{-1} + \tanh[kL]},$$
$$C_L(k) = -\frac{k^{-1}\sqrt{G}\tanh[kL] + (K-1)}{k^{-1}\kappa \tanh[kL] + K}.$$

Plugging into (4.6) with $g_0(z,t) = S_0(z,t)$, $g_1(z,t) = S_1(z,t)$, we obtain

$$\dot{h}_1 = \omega(k) h_1$$

with

$$\omega(k) = \bar{S}_I \left(1 - \frac{k}{\sqrt{G}} + \frac{C_L(k)\sqrt{G}}{\kappa + k} \right).$$

Several dispersion curves are shown in Figure 3 for increasing values of G. Note that the most unstable wavenumber increases like $G^{1/2}$.

5. 2D nonlinear evolution. Linear theory aside, the biofilm model presented is in fact nonlinear, the important nonlinearity being due to the moving interface. Hence we now study the full model system computationally in order to follow the nonlinear evolution of fingering instabilities. For convenience, we make several changes to the previous setup. The biofilm will no longer be infinitely deep but rather will be contained in a 2D box, periodic in the horizontal direction. The biofilm will grow from the bottom of the box, $z = 0$, toward the bulk fluid at $z = H$. $H = H(t)$ is chosen to be a given length L above the maximum interface height. We label the fluid region of the box by Ω_1 and the biofilm region of the box by Ω_2. The regions Ω_1 and Ω_2 are separated by the interface curve $\boldsymbol{\gamma}$. We choose the simple usage function $u(S) = S$ and growth function $g(S) = u(S) - \mu = S - \mu$, again taking the point of view that small S_∞ calculations are of most interest here, and hence a general choice of $u(s)$ and $g(S)$ may be replaced by their linearizations around $S = 0$. The new parameter $\mu \geq 0$ is introduced as a maintenance cutoff level. Where $S > \mu$, the biofilm grows; where $S < \mu$, the biofilm suffers necrotic decay. This is essentially a computational

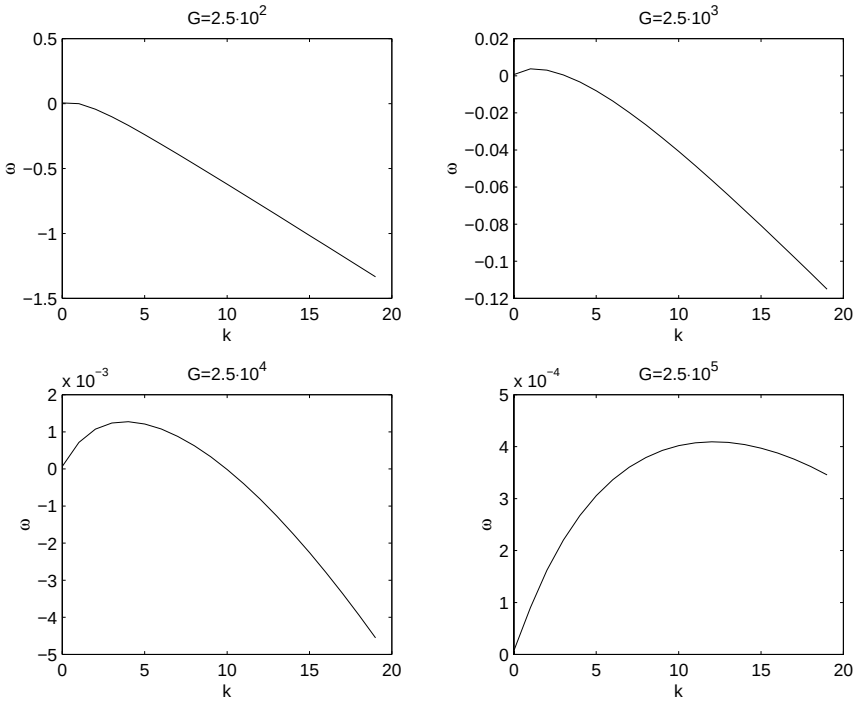

FIG. 3. *Dispersion diagrams for increasing values of G with $K = 8$, $L = 2$, and $u(S) = g(S) = S$.*

convenience—we include necrosis in order that the biofilm interface remains within our computational domain. While there is some experimental evidence [6] that subactive layer necrosis plays a role in biofilm evolution, and, certainly, biofilms do not expand indefinitely, loss mechanisms in laboratory biofilms are not presently well understood.

Altogether then, the model equations to be solved are

$$\begin{aligned} \nabla^2 p &= -S + \mu, \qquad (x,z) \in \Omega_2, \\ D_i \nabla^2 S &= \begin{cases} 0, & (x,z) \in \Omega_1, \\ S, & (x,z) \in \Omega_2, \end{cases} \end{aligned} \tag{5.1}$$

with interface normal velocity $-\mathbf{n} \cdot \nabla p|_{\boldsymbol{\gamma}^-}$. The boundary and interface conditions are $p_z|_{z=0} = S_z|_{z=0} = 0$, $p|_{\boldsymbol{\gamma}} = 0$, $S|_{\boldsymbol{\gamma}^+} = S|_{\boldsymbol{\gamma}^-}$, $D_1 \mathbf{n} \cdot \nabla S|_{\boldsymbol{\gamma}^+} = D_2 \mathbf{n} \cdot \nabla S|_{\boldsymbol{\gamma}^-}$, and $S|_{z=H} = 1$. These equations again have 1D moving front solutions, although now with the possibility of approaching an equilibrium $h(t) = h_{eq}$ due to the cutoff parameter μ. Linear stability analysis around these 1D solutions may be performed as before. We refer to the appendix for the actual front and linearization solutions.

System (5.1) is solved numerically on a uniform 2D rectangular grid, with periodic boundary conditions on the side, no-flux conditions on the bottom, and Dirichlet conditions at $z = H$ (or on the interface, in the case of the pressure equation). The interface is tracked implicitly using a level set function $\phi(x, z, t)$ (see [23]) implemented as in [25]. We present a brief outline of the method here; the reader is directed to the references for further details. The interface is given by the level set $\phi = 0$. The value of ϕ at a given grid point is the signed distance of that point from the interface. A single iterative step proceeds as follows. First, the substrate equation is

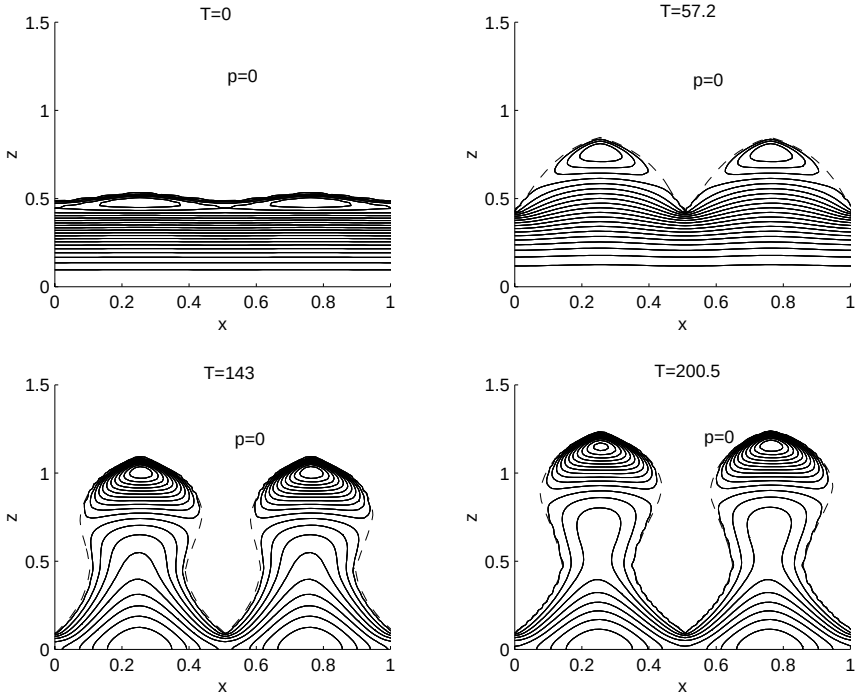

FIG. 4. *Pressure contours for an evolving biofilm. The dashed lines are the interfaces* $\phi = 0$. *The bubble regions formed after the initial time are the regions of positive pressure.*

solved with the piecewise constant diffusion coefficient smoothed near the interface. Next, the pressure equation is solved in the biofilm region. The level set function is then advected as a passive scalar using the velocity field $-\nabla p$. Above and near the interface, an advection velocity field is constructed by linearly extending the pressure across the interface. This extension is smoothed to zero away from the interface. Finally, the newly advected level set function ϕ is renormalized to signed distance from the interface, typically after each time step.

See Figure 4 for the pressure contours of a typical example of unstable evolution. The dispersion relation for the initial conditions corresponding to Figure 4 is shown in Figure 5. Recall that the ambient pressure is set to 0 so that, in the figure, the interface between biofilm and fluid lies on the envelope (dashed line) of the pressure contours. The bubbles on the tips of the growing fingers are the regions of positive pressure where most growth is occurring. The rest of the biofilm is at negative pressure and is actually slowly contracting. We seem to observe that, rather than tip-splitting or dendritic evolution, the initial thin active layer evolves after finger formation into blobs that eventually become mushrooms. This is perhaps not surprising since the finger width and biofilm penetration depth are both $O(G^{-1/2})$, suggesting that the active layer may coalesce into an active bubble on the ends of biofilm fingers, thus suppressing further fingering.

6. Discussion. The structural mechanics of biofilms are important yet poorly understood even on a simple level. In this paper we have developed a single substrate model to address the most basic of structural questions, unstressed biofilm growth and mushroom formation. Our model follows a number of CA models on the subject

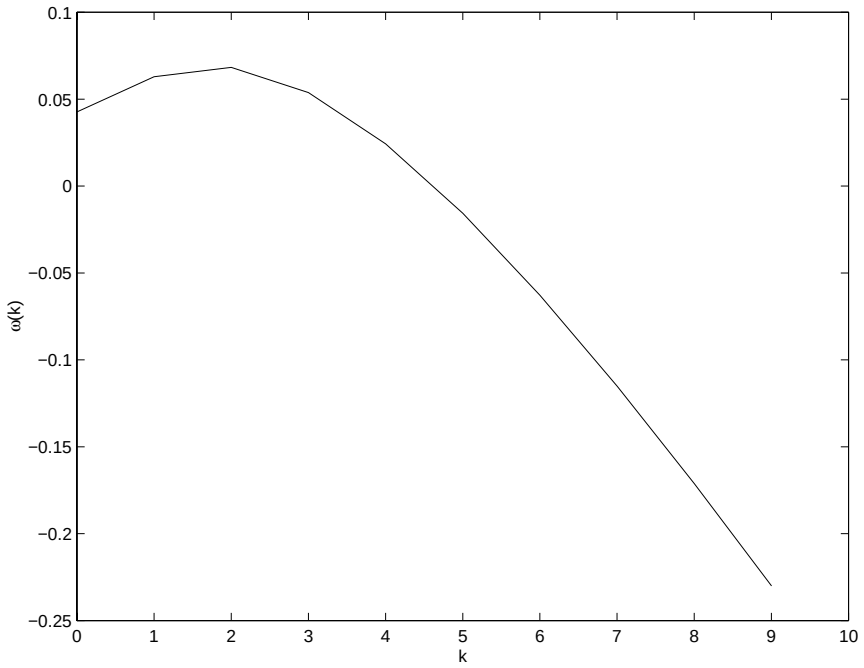

FIG. 5. *Dispersion diagram for the numerical example. Here* $L = .15$, $K = 5$, $\mu = .01$, *and* $G = 1000$.

and shares the common feature of exhibiting increasingly fine structure with decreasing substrate supply. Because our continuum model is amenable to linear stability analysis, we are able to provide scaling predictions of this process that can be compared to experimental data. The central conclusion of the presented results is that, for a robust class of biofilm systems, both growth rate (for flat biofilms) and spatial structure (for heterogeneous biofilms) are predicted to scale like $G^{-1/2}$.

The reader should certainly be aware that there are at least two important contributors to biofilm structure that have not been included in the present model. First, at least in the laboratory, most biofilm systems include fluid flow. Fluid dynamics introduces improved substrate transport and fluid stress. Experimental evidence would seem to indicate that strong fluid shear stress significantly influences biofilm sloughing and biofilm structure in general. Second, there is increasing experimental evidence of the importance of internal chemical signaling in biofilm growth and behavior. It is conjectured that such processes may have a wide influence on, for example, biofilm growth, decay, and structural integrity. Both of these additional factors may very well have important effects on biofilm structure. It should be noted, however, that it is not necessary to appeal to them in order to explain the complicated geometries that can be found in biofilms. Those may be explainable simply from fundamental growth processes, as argued here.

On a broader level, the fingering instability presented here seems to be yet another variation in a growing class of unstable interface problems. It has the two key balancing ingredients of such an instability. First, the fingering process itself favors short wavelength structure through, essentially, improved access to substrate. A second process, growth-induced pressure from below, favors long wavelength structure

while regularizing the interface. The two mechanisms combine to determine a preferred wavelength. We note that there is no need to appeal to surface tension to regularize this problem; regularization is already achieved by growth pressure. This self-regularization apparently may also result in inhibition of finger splitting, an observation, however, based only on numerics arising from a specific choice of biology functions u and g and at relatively low G.

7. Appendix. Analytical solution of the linearized box system. Equations (5.1) have 1D solution $S_0 = S_0(z,t)$, $p_0 = p_0(z,t)$, and $h_0 = h_0(t)$ where, setting $\bar{S}_I = (1 + K^{-1}L\sqrt{G}\tanh(\sqrt{G}h_0))^{-1}$ as the interface substrate concentration,

$$S_0(z,t) = \begin{cases} 1 - \bar{S}_I K^{-1}\sqrt{G}\tanh(\sqrt{G}h_0)(H-z), & h_0 < z < H, \\ \bar{S}_I(\cosh[\sqrt{G}(h_0-z)] - \tanh(\sqrt{G}h_0)\sinh[\sqrt{G}(h_0-z)]), & 0 < z < h_0, \end{cases}$$

$$p_0(z,t) = \bar{S}_I G^{-1}\left(1 - \cosh[\sqrt{G}(h_0-z)] + \tanh(\sqrt{G}h_0)\sinh[\sqrt{G}(h_0-z)]\right)$$

$$+ \frac{\mu}{2}(z^2 - h_0^2), \qquad 0 < z < h_0, \tag{7.1}$$

with

$$\dot{h_0} = -p_z|_{z=h_0} = \bar{S}_I G^{-1/2}\tanh(\sqrt{G}h_0) - \mu h_0. \tag{7.2}$$

Note that for $\mu = 0$ this solution rapidly approaches the infinite depth solution (3.4)–(3.6), as soon as the biofilm depth h exceeds the active layer thickness $G^{-1/2}$. For shallow biofilms, i.e., $h_0 < G^{-1/2}$, note that $\dot{h}_0 \approx (\bar{S}_I - \mu)h_0 = g(h_0)h_0$.

To perform a linear stability analysis, as before assume S, p, and h to be of the form

$$\begin{aligned} S(z,y,z,t) &= S_0(z,t) + S_1(z,t)\exp(i\mathbf{k}\cdot\mathbf{x}), \\ p(z,y,z,t) &= p_0(z,t) + p_1(z,t)\exp(i\mathbf{k}\cdot\mathbf{x}), \\ h(z,y,t) &= h_0(t) + h_1(t)\exp(i\mathbf{k}\cdot\mathbf{x}), \end{aligned}$$

where S_0, p_0, and h_0 are the above solutions of the 1D problem, and then solve for S_1, p_1, and h_1 to first order. After some algebra we arrive at

$$S_1(z,t) = \begin{cases} C_U\bar{S}_I\sqrt{G}\frac{\sinh[k(H-z)]}{\cosh[k(H-h_0)]}h_1(t), & h < z < H, \\ C_L\bar{S}_I\sqrt{G}\frac{\cosh[\kappa z]}{\cosh[\kappa h_0]}h_1(t), & 0 < z < h, \end{cases}$$

where $\kappa^2 = k^2 + G$ and

$$C_U = \frac{-k^{-1}\sqrt{G} + k^{-1}\kappa(1-K^{-1})\tanh[\sqrt{G}h_0]\tanh(\kappa h_0)}{k^{-1}\kappa\tanh[k(H-h_0)]\tanh[\kappa h_0] + K},$$

$$C_L = -\frac{k^{-1}\sqrt{G}\tanh[k(H-h_0)] + (K-1)\tanh(\sqrt{G}h_0)}{k^{-1}\kappa\tanh[\kappa h_0]\tanh[k(H-h_0)] + K}.$$

The solution for p_1 is

$$p_1(z,t) = \frac{\cosh(kz)}{\cosh(kh_0)}\left(k^{-1}\int_0^{h_0} S_1(s,t)\sinh[k(h_0-s)]ds - p_{0,z}(h_0,t)h_1(t)\right)$$

$$-k^{-1}\int_0^z S_1(s,t)\sinh[k(z-s)]ds,$$

and then

$$\begin{aligned}\dot{h}_1 &= -p_{0,zz}(h_0,t)h_1 - p_{1,z}(h_0,t)\\ &= h_1\left[\bar{S}_I - \mu - k\tanh(kh_0)(G^{-1/2}\bar{S}_I\tanh(\sqrt{G}h_0) - \mu h_0)\right]\\ &\quad - \tanh(kh_0)\int_0^{h_0} S_1(s,t)\sinh[k(h_0-s)]ds + \int_0^{h_0} S_1(s,t)\cosh[k(h_0-s)]ds.\end{aligned}$$

Evaluating, we obtain $\dot{h}_1 = \omega(k)h_1$, where

$$\begin{aligned}\omega(k) = \bar{S}_I(1 - kG^{-1/2}\tanh(kh_0)\tanh(\sqrt{G}h_0)) + \mu(kh_0\tanh(kh_0) - 1)\\ + \frac{C_L\bar{S}_I}{2\sqrt{G}}(1-\tanh(kh_0))\left[\kappa\tanh(\kappa h_0) + k\left(1 - \frac{2\exp(kh_0)}{\cosh(\kappa h_0)}\right)\right]\\ + \frac{C_L\bar{S}_I}{2\sqrt{G}}(1+\tanh(kh_0))\left[\kappa\tanh(\kappa h_0) - k\left(1 - \frac{2\exp(-kh_0)}{\cosh(\kappa h_0)}\right)\right].\end{aligned}$$

When h_0 is large (compared to the active layer width $G^{-1/2}$ and the perturbation scale k^{-1}) this expression reduces to

$$\omega(k) \approx \bar{S}_I(1 - kG^{-1/2}) + \mu(kh_0 - 1) + \frac{C_L\sqrt{G}\bar{S}_I}{\kappa + k},$$

the same as the infinite layer solution when $\mu = 0$.

Acknowledgments. The authors would like to thank M. Pernarowski, N. Cogan, and P. Stoodley for their assistance.

REFERENCES

[1] P. Alberch, G. M. Odell, G. F. Oster, and B. Burnside, *The mechanical basis of morphogenesis*, Develop. Biol., 85 (1981), pp. 446–462.
[2] M. Ballyk and H. Smith, *A model of microbial growth in a plug flow reactor with wall attachment*, Math. Biosci., 158 (1999), pp. 95–126.
[3] E. Ben-Jacob, O. Schochet, A. Tenenbaum, I. Cohen, A. Czirok, and T. Vicsek, *Generic modelling of cooperative growth patterns in bacterial colonies*, Nature, 368 (1994), pp. 46–49.
[4] H. M. Byrne, *A weakly nonlinear analysis of a model of avascular tumor growth*, J. Math. Biol., 39 (1999), pp. 59–89.
[5] M. A. J. Chaplain, *Avascular growth, angiogenesis and vascular growth in solid tumours: The mathematical modelling of the stages of tumour development*, Math. Comput. Modelling, 23 (1996), pp. 47–87.
[6] W. G. Characklis, *Kinetics of microbial transformations*, in Biofilms, W. G. Characklis and K. C. Marshall, eds., Wiley, New York, 1990, pp. 233–264.
[7] R. L. Chuoke, P. Van Meurs, and C. Van der Pol, *The instability of slow, immiscible, viscous liquid-liquid displacements in permeable media*, Trans. AIME, 216 (1959), pp. 188–194.
[8] E. A. Coddington and N. Levinson, *Theory of Ordinary Differential Equations*, McGraw–Hill, New York, 1955.
[9] J. W. Costerton, *Overview of microbial biofilms*, J. Indust. Microbiol., 15 (1995), p. 137.
[10] J. W. Costerton, Z. Lewandowski, D. E. Caldwell, D. R. Korber, and H. M. Lappin-Scott, *Microbial biofilms*, Annu. Rev. Microbiol., 49 (1995), pp. 711–745.
[11] R. Dillon, L. Fauci, A. Fogelson, and D. Gaver, *Modeling biofilm processes using the immersed boundary method*, J. Comput. Phys., 129 (1996), pp. 57–73.
[12] H. J. Eberl, D. F. Parker, and M. C. M. van Loosdrect, *A new deterministic spatio-temporal continuum model for biofilm development*, J. Theor. Med., 3 (2001), pp. 161–175.

[13] H. P. Greenspan, *On the growth and stability of cell cultures and solid tumors*, J. Theor. Biol., 56 (1976), pp. 229–243.
[14] W. Gujer and O. Wanner, *Modeling mixed population biofilms*, in Biofilms, W. G. Characklis and K. C. Marshall, eds., Wiley, New York, 1990, pp. 397–443.
[15] P. Harremoes, *Biofilm kinetics*, in Water Pollution Microbiology, Vol. 2, R. Mitchell, ed., Wiley, New York, 1978, pp. 71–109.
[16] S. W. Hermanowicz, *A simple* $2D$ *biofilm model yields a variety of morphological features*, Math. Biosci., 169 (2001), pp. 1–14.
[17] W. W. Mullins and R. F. Sekerka, *Stability of a planar interface during solidification of a dilute binary alloy*, J. Appl. Phys., 3 (1964), pp. 444–451.
[18] J. D. Murray, G. F. Oster, and A. K. Harris, *Mechanical aspects of mesenchymal morphogenesis*, J. Embryol. Exp. Morph., 78 (1983), pp. 83–125.
[19] P. Pelce, *Dynamics of Curved Fronts*, Academic Press, Boston, 1988.
[20] C. Picioreanu, M. C. van Loosdrecht, and J. J. Heijnen, *Two-dimensional model of biofilm detachment caused by internal stress from liquid flow*, Biotechnol. Bioeng., 72 (2001), pp. 205–218.
[21] C. Picioreanu, J. Heijnen, and M. C. M. van Loosdrecht, *Mathematical modeling of biofilm structure with a hybrid differential-discrete cellular automaton approach*, Biotechnol. Bioeng., 58 (1998), pp. 101–116.
[22] P. G. Saffman and G. I. Taylor, *The penetration of a fluid into a porous medium or Hele–Shaw cell containing a more viscous liquid*, Proc. Roy. Soc. London Ser. A, 245 (1958), pp. 312–329.
[23] J. A. Sethian, *Level Set Methods*, Cambridge University Press, Cambridge, UK, 1996.
[24] P. Stoodley, D. deBeer, J. D. Boyle, and H. M. Lappin-Scott, *Evolving perspectives of biofilm structure*, Biofouling, 14 (1999), pp. 75–94.
[25] M. Sussman, *A Level Set Approach for Computing Solutions to Incompressible Two-Phase Flow*, Ph.D. thesis, Department of Mathematics, UCLA, CAM Report 94-13, 1994.
[26] J. W. T. Wimpenny, *Microbial systems: Patterns in space and time*, Adv. Micro. Ecol., 12 (1992), pp. 469–522.